Int. J. Electrochem. Sci., 10 **(2015)** 8691 - 8705

International Journal of
ELECTROCHEMICAL
SCIENCE
www.electrochemsci.org

The Corrosion Behavior of Magnesium Alloy AZ31 in Hot and Dry Atmospheric Environment in Turpan, China

Cheng Man[1], *Chaofang Dong*[1,*], *Yuehua Fang*[3], *Kui Xiao*[1], *Chunyun Guo*[3], *Gang He*[3], *Xiaogang Li*[1,2]

[1] Corrosion and Protection Center, Key Laboratory for Corrosion and Protection (MOE),, University of Science and Technology Beijing, Beijing 100083, China
[2] Ningbo Institute of Material Technology & Engineering, Chinese Academy of Sciences, Ningbo 315201, Zhejiang, Peoples R China.
[3] Xinjinang Turpan Natural Environmental Test Research Center, Xinjinang Turpan 838200
[*]E-mail: cfdong@ustb.edu.cn

Received: 20 July 2015 / *Accepted:* 12 August 2015 / *Published:* 26 August 2015

The corrosion behavior of magnesium alloy AZ31 in the hot and dry atmospheric environment was investigated. The results showed that the electrochemical process was hindered and the intergranular corrosion was the main degraded mechanism in this condition. The dominate corrosion product during the exposure time was $Mg_5(CO_3)_4(OH)_2 \cdot 0.5H_2O$, and the product layer reduced the corrosion rate. The content of aluminum was higher in the product layer than that of the substrate. The electrochemical measurements revealed that the influence of the layer mainly on the anodic procedure.

Keywords: Magnesium alloy; Hot and dry atmosphere; intergranular corrosion; Rust

1. INTRODUCTION

Magnesium alloys have been widely used in the transport sector and other industries due to its low density, which could contribute to energy saving and reduced environment impact [1-5]. For example, the use of magnesium in cars could lead to significant weight reduction, by about 60 %. Meanwhile, the greenhouse gas emissions reduced by 100 kg over the lifetime of the vehicle [3]. However, the poor corrosion resistance of magnesium alloys is one of the most important reasons that hamper their applications[6]. Therefore, in order to provide the basis for magnesium applications, it is necessary to study the corrosion behavior of magnesium alloys in the atmosphere.

In recent years, a series of studies on the corrosion behavior of magnesium alloys in different atmospheric environments have been carried out by the actual atmospheric exposure and laboratory simulation tests [1, 3, 7, 8]. Martin et al. [7] reported that the main corrosion product formed on

AZ91D was magnesium carbonate hydromagnesite ($Mg_5(CO_3)_4(OH)_2 \cdot 4H_2O$) at all the urban, rural and marine exposure sites, and the largest corrosion rate appeared in the marine atmospheric environment due to the higher relative humidity and the content of chloride ions. Scholars [9, 10] studied the influence of CO_2 on the corrosion resistance of magnesium alloys, and the results revealed that (i) the dry mass gain of the samples exposed to CO_2-free air was approximately four time greater than that of exposed to the presence of CO_2; and (ii) the passivating magnesium hydroxide film formed in the former environment didn't provide efficient protection, whereas the film formed in the latter condition, mainly consisted of magnesium carbonate hydromagnesite, hindered the cathode and anode reactive. Song et al. [11] studied the effect of the humidity and temperature on the corrosion behavior of magnesium alloys using an environmental simulation system, and reported that the degradation process of the sample surfaces was accelerated at a higher environment temperature or higher relative humidity. The authors [11] also reported that there were two mechanisms of corrosion process: oxidation and electrochemical corrosion, andthe electrochemistry corrosion should be faster than the oxidation process at a temperature lower than 100℃.

Aluminum is one of the most important alloying elements for magnesium. It is a common theory that the addition of aluminum results in the enhancement of the corrosion resistance of magnesium alloys [3, 8, 12]. aluminum inhibited the corrosion of magnesium alloys by two steps [3, 13]: (i) the phase enrichment in aluminum acted as an electrochemical barrier for corrosion progression and (ii) the formation of a semi-protective Al-rich oxide layer near the substrate reduces the corrosion susceptibility. What's more, the distribution of aluminum could also impact on the deteriorate rate of magnesium alloys [3, 8, 14, 15].

Although lots of studies have been carried out in different atmospheric environments, there was little attention paid onto the hot and dry environment like Turpan in the northwest of China. The atmospheric environment that belongs to a continental dry tropical desert climate was characterized by a large temperature difference between day and night, a longtime sunshine, and a low relative humidity [16].

In the present work, the corrosion behavior of AZ31 magnesium alloys exposed to the hot and dry atmospheric environment for three years was investigated. The corrosion rate was determined by the weight loss method. The composition and structure of the corrosion product was analyzed by X-ray spectroscopy (EDS), X-ray diffraction (XRD) and X-ray photoelectron spectroscopy (XPS), and its protectiveness was evaluated using electrochemical methods. The corrosion process was also discussed in this work.

2. EXPERIMENTS

2.1. Material

The material used in the present work was commercial magnesium alloy AZ31. The nominal chemical composition (wt. %) was listed in Table 1. As shown in Fig. 1, there were a few Al-Mn intermetallic particles appearing in the grains and at grain boundaries (dark area in Fig. 1). The

microstructure of AZ31 was single phase, and the grain size was in the range of 5~50 μm. The samples with size of 150 mm × 75 mm × 3 mm were cut from a sheet. Then all the surfaces of the samples were polished with emery paper up to 800 grits, rinsed with distilled water, degreased with acetone and dried. The samples were installed on a test rack with an inclination of 45º, and exposed to the natural environment in Turpan for three years. Three replicas were used to calculate the weight loss of samples, and the others were prepared for studying the corrosion process, corrosion morphology and corrosion product.

Table 1. The nominal chemical composition of the magnesium alloy AZ31 used.

Alloy	Chemical composition (wt. %)							
	Al	Zn	Mn	Si	Fe	Cu	Ni	Mg
AZ31	3.19	0.81	0.30	0.025	0.006	0.002	0.0006	Bal.

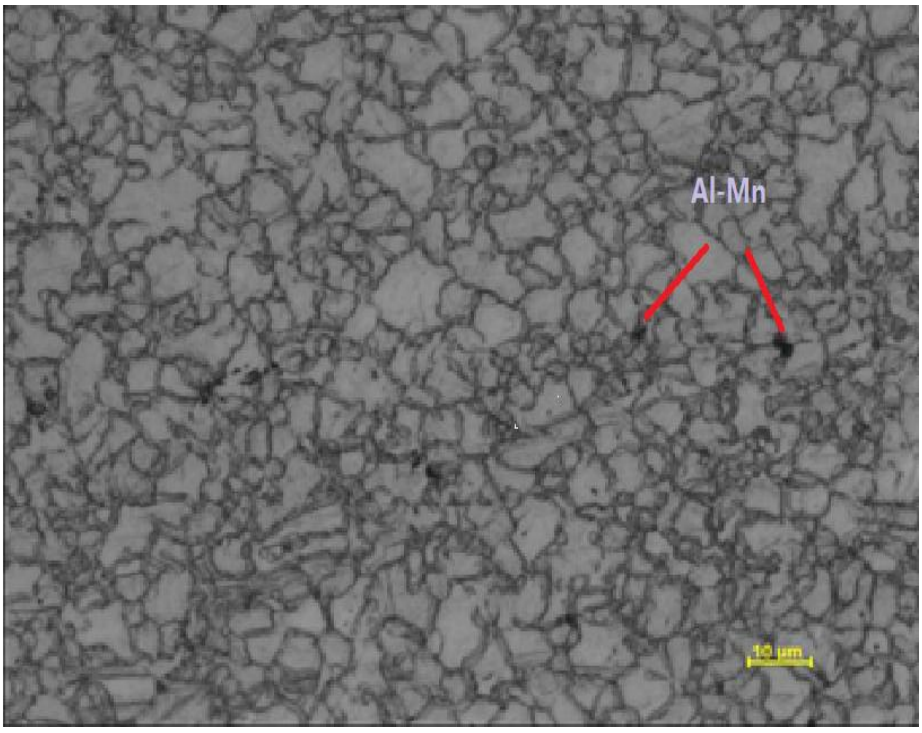

Figure 1. The microstructure of AZ31 magnesium alloy used

2.2. Environment conditions of the exposure site

The meteorological parameters during the first exposure year in Turpan, China were listed in Table 2. The average temperature and the average relative humidity during the first year were 15℃ and 31.3%, respectively. The annual total radiation and the total sunshine period were 5,513 MJ/m^2 and 3,200 h, respectively. The most remarkable characteristic is the temperature difference between day and night, which could be up to dozens of degrees.

Table 2. The meteorological data of Turpan exposure station (2012-07~2013-06)

Data	2012						2013					
	7	8	9	10	11	12	1	2	3	4	5	6
Average temperature / ℃	35.8	33.8	27.1	16.3	1.6	-6.7	-12.6	1.5	16.4	23.0	28.9	33.2
Average highest temperature / ℃	39.8	39.2	32.8	25.2	6.2	-2.6	-7.2	6.0	20.6	27.0	32.0	37.7
Average lowest temperature / ℃	30.4	28.4	21.5	11.2	-2.1	-9.9	-16.4	-2.9	7.7	14.1	20.9	28.6
Precipitation / mm	0.0	0.0	0.0	0.0	0.0	0.0	0.00	0.00	0.00	0.02	0.00	0.00
Average relative humidity / %	21	14	20	26	30.1	59.3	80.0	42.8	17.4	15.1	14.1	18.3
Average wind speed / $m \cdot s^{-1}$	3.4	3.7	2.2	2.4	2.5	1.5	1.0	2.0	2.1	2.6	3.3	4.1

2.3. Weight loss measurement

Corrosion products formed on the withdraw samples were removed by immersing in a specific medium (200 g/L CrO_3 + 10 g/L $AgNO_3$) for 1 min at ambient temperature (GB/T 16545 - 1996). The corrosion rate was calculated using equation (1) [2, 7, 17].

$$v_1 = (w_0 - w_1) / (S * t) \quad (1)$$

Where v_1 was the corrosion rate ($g \cdot m^{-2} \cdot a^{-1}$), w_0 and w_1 were the origin and the final weight (g), S was the surface area (m^2), and t was the exposure time (year).

2.4. Corrosion products analysis and morphology observation

The composition of the corrosion products formed on the exposed specimens was examined using EDS, XRD and XPS. After removing the corrosion products, the surface and cross-section were observed by a scanning electron microscopy (SEM, Quata 250).

2.5. Electrochemical measurements

Electrochemical measurements were carried on a VMP3 electrochemical workstation in the solutions saturated with $Mg(OH)_2$ (with/without 0.1M NaCl) in a conventional three-electrode cell, where the platinum acted as the counter electrode and a saturated calomel electrode (SCE) as the reference electrode. Several circles with a radius of 10mm selected from the surface of the withdraw specimens served as the working electrode surfaces.

Potentiodynamic polarization curves were measured in the range from 0.3 V_{OCP} (versus the open circle potential (OCP)) to 0.5 V_{OCP} with a scanning rate of 0.333 mV/s. Electrochemical impendence spectroscopy (EIS) measurements were performed over a frequency ranging from 100 kHz to 10 mHz using a 10 mV amplitude sinusoidal voltage. The EIS data were analyzed by

commercial software ZsimpWin. All the electrochemical experiments were carried out at room temperature and repeated at least three times to maintain the reproducibility.

The samples used in electrochemical experiment were the alloys after exposed in Turpan, China and the specimens after removing the rust and polishing with 60, 150, 400, 800, 1500 grits emery paper. The samples were represented with *Covered* and *Substrate*, respectively in this paper.

3. RESULTS

3.1. Corrosion test

The average corrosion rate ($g \cdot m^{-2} \cdot a^{-1}$) of the specimens exposed in Turpan for three years was about 2.17 $g \cdot m^{-2} \cdot a^{-1}$, which was smaller than that of the specimens exposed for one year (about 3.90 $g \cdot m^{-2} \cdot a^{-1}$). Correspondingly, the corrosion rates were 2.24 and 1.25 μm/a for one-year specimen and three-year specimen, according to the following equation:

$$v_2 = \frac{1}{\rho} \qquad (2)$$

Where v_2 was the corrosion rate (μm/a) and ρ was the density of the magnesium alloy. The rate was times larger than aluminum alloys (7A04, 2A12), the corrosion rates in the first exposure year of which were 0.47 and 0.21μm/a in the same atmospheric environment, respectively [16]. The magnesium alloy AZ31 exhibited better corrosion resistance than carbon steel (37.2 μm/a for Q235 and 34.6 μm/a for Q450 in the first exposure year) [18]. Cui et.al [2] studied the corrosion behavior of magnesium alloy AZ31 exposed to the typical marine atmospheric condition at Xisha Island , and revealed that the average corrosion rate of AZ31 was about 17.66 μm/a in the first exposure year. The difference in the corrosion behavior between the two types of atmospheric environments will be discussed later.

3.2. Morphology observation

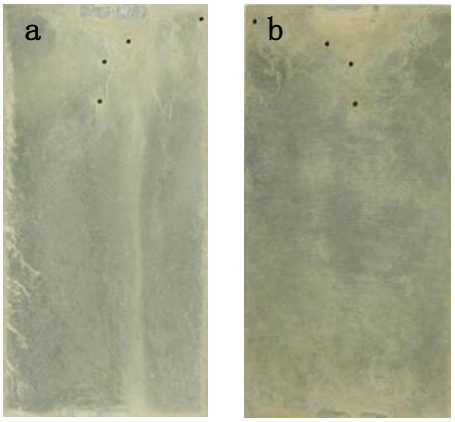

Figure 2. The Macro-morphology of an AZ31 specimen exposed in Turpan for three years: (a) front face; (b) back face

Fig. 2 showed the macro-morphology of an AZ31 specimen after exposed in Turpan for three years. The front face of the specimen was covered by a layer of gray corrosion products and the appearance of the back face is similar to that of the front face, but the color was darker. The difference in color between the faces was caused by the sand and the some white corrosion product deposition.

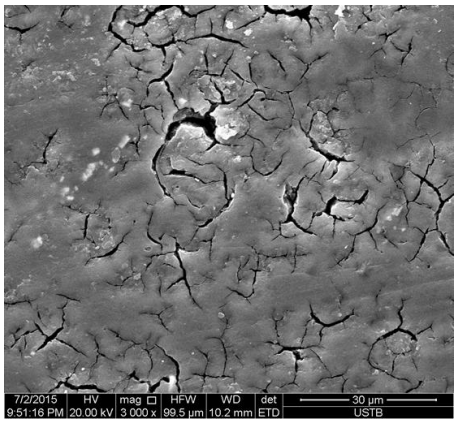

Figure 3. The micro-morphology of a magnesium alloy AZ31 specimen exposed in Turpan for three years

The morphology of corrosion products on AZ31 specimens after exposed in Turpan for three year was obtained with SEM. As shown in Fig. 3, the surface of the corrosion products consisted of high density of cracks and compact area. Some cracks were wider and deeper, which might be able to result in localized corrosion. Those cracks which would decrease the protective of the product layer was due to the Pilling-Bedworth ratio (P-B ratio) of magnesium was lower than 1 [19]. Different from this work, Cui et.al [2] reported that there were numerous acicular clusters appearing on the surface of the AZ31 exposed for 12 and 24 months. The reason for the difference might be due to the hot and dry atmosphere in Turpan.

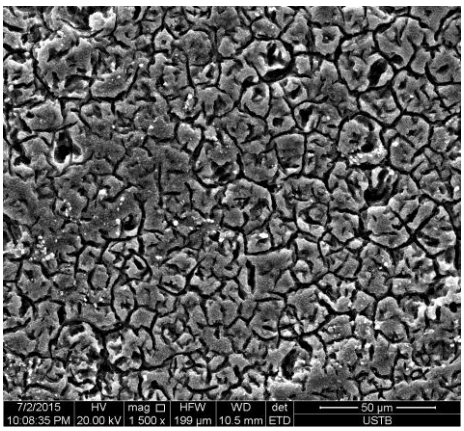

Figure 4. The morphology of a AZ31specimen exposed for three years in Turpan after removing the corrosion products

Fig. 4 presents that after removing the corrosion products, there were a large number of ditches spreading on the surfaces and some pits at the junctions of the ditches of the three-year AZ31 specimens. since the grain boundaries of AZ31 were preferred to be attacked by aggressive species [1], these pits manifested that intergranular corrosion was one of the main mechanisms of AZ31 failure [12]. The morphology displayed in Fig.4 was different from those reported in previous literature where the surfaces of magnesium alloys exposed to the marine atmospheric environment and the simulate conditions was embedded by pits [2, 3, 9, 20, 21]. Song et.al [11] reported that in the dry atmospheric environment, the electrochemical procedure that leaded to pits would be restrained. Meanwhile, during exposed in the hot and dry condition, a large ohmic potential drop in the thin water layer on the surface of the specimen would decrease the possibility of galvanic coupling of alloy constituents [7].

3.3. Corrosion products analysis

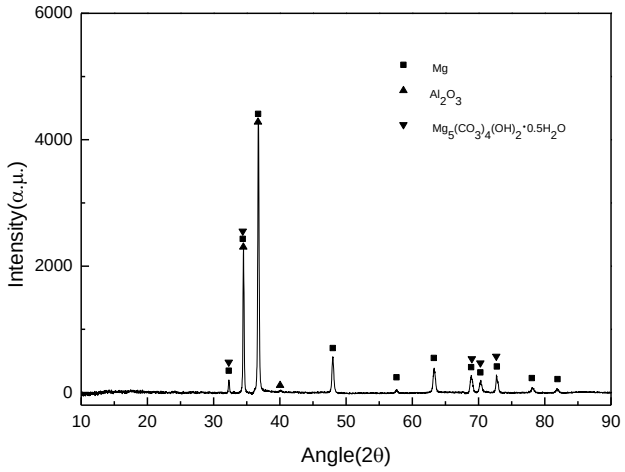

Figure 5. The XRD pattern of the corrosion products formed on an AZ31 specimen after exposed in Turpan for three years

The main compositions of the corrosion products formed on AZ31 specimens exposed in Turpan for three years was analyzed by XRD and XPS. As plotted in Fig. 5, one of the primarily contents of the corrosion products was the carbon-containing pokroskite ($Mg_5(CO_3)_4(OH)_2 \cdot 0.5H_2O$), where the bounding water was less than that in the hydromagnesite ($Mg_5(CO_3)_4(OH)_2 \cdot 4H_2O$) which formed on the magnesium alloys exposed in the marine atmospheric environment [1, 2, 7, 17]. The carbon-containing compounds with compact structure were able to prevent the active species from attacking the material, which had been confirmed by other scholar [9]. As shown in Fig. 5, the characteristic peaks representing Al_2O_3 appeared in this XRD pattern. The XPS displayed in Fig. 8 revealed that the products would had larger content of aluminum than the substrate, and the element existed in a form of Al2O3 that acted as a protective layer in the samples, because Magnesium was more preferable to deviate from the magnesium alloy AZ31 than aluminum when the alloy was exposed in Turpan atmospheric condition [3].

Fig. 6 shows the XPS spectra of an AZ31 specimen after exposure for three years in Turpan. The high resolution spectra of the three main elements (Fig. 6(b), Fig. 6(c) and Fig. 6(d)) revealed that the products consisted of carbides, oxides, hydroxides and their mixtures, and the carbides were the most abundant ingredients. The Al_2O_3 (77.26 eV), the main form of aluminum, was also detected, which was consistent with the results of XRD. Additionally, the XPS demonstrated that trace of chloride appeared in the corrosion products, which might result from the deposition.

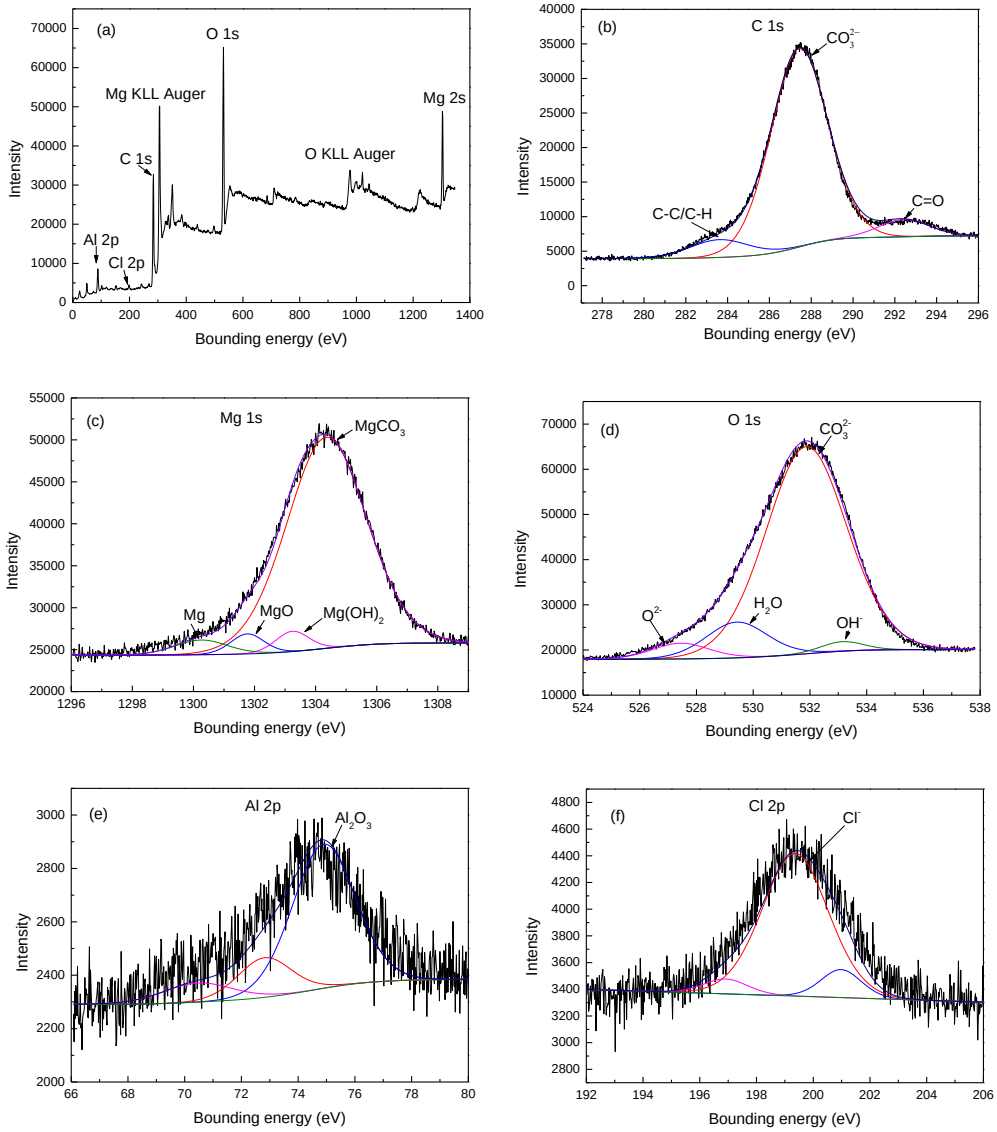

Figure 6. The XPS analysis of the corrosion products formed on a AZ31 specimen after exposure in Turpan for three years: (a) the whole spectra after etching 30 s; (b)-(f) the high resolution spectra of C 1s, Mg 1s, O 1s, Al 2p and Cl 2p after etching 30 s, respectively

Fig. 7 presents the whole spectra of the product layer developed on the AZ31 during exposure for three years in Turpan. The two spectroscopies (etching 30 s, and 10 min) presented different depths. The compositions of the corrosion products in the two positions were exhibited in Fig. 8. The carbon content in the deeper site was higher than the other one (At.% 49.94 and 25.12, respectively).

The Al/Mg ratios were 0.14 for the outer layer, 0.08 for the inner layer and 0.03 for the substrate, respectively.

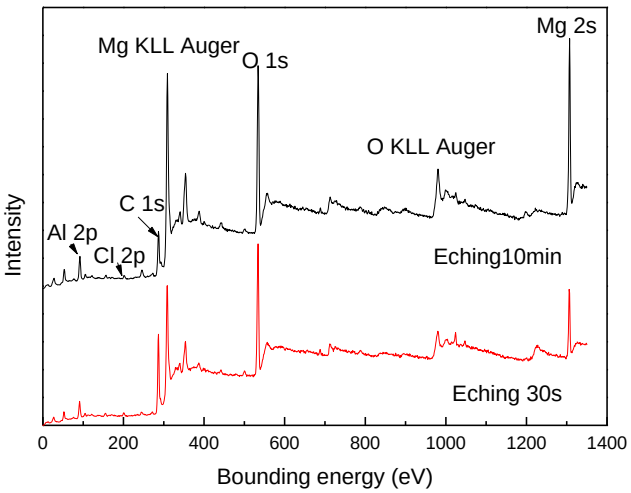

Figure 7. The XPS spectra for different etching times of the corrosion products formed on the AZ31 after exposure in Turpan for three years

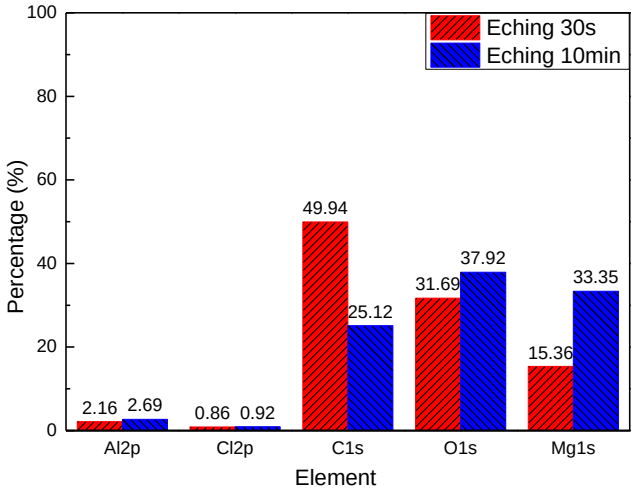

Figure 8. The element contents for etching different times of the corrosion products formed on the AZ31 after exposure in Turpan for three years

3.4. Electrochemical measurements

3.4.1 Potentiodynamic polarization

Fig. 9(a) presents the polarization curves of the covered specimen and the substrate in the saturated $Mg(OH)_2$ solution with 0.1M NaCl, where covered specimens represented the with corrosion products and the substrate was behalf of the samples without corrosion products. Both obtained curves showed similar cathodic polarization behavior - hydrogen evolution reaction [2, 22], whereas the anodic part of the curves clarified that there were obvious differences between the substrate of AZ31 and the samples covered by corrosion products. The plot of the covered specimen demonstrated the

passive characteristic, by presenting a relatively stable current density between around -1.4 to -1.218 V_{SCE}.

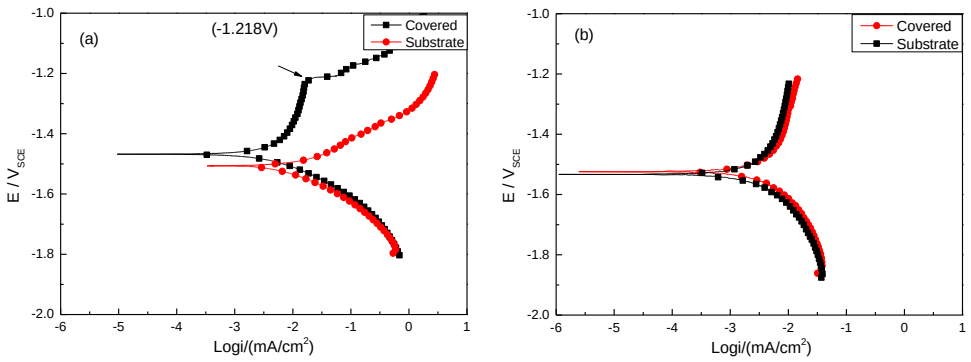

Figure 9. The potentiodynamic polarization curves of AZ31 specimens in the solutions with saturated $Mg(OH)_2$: (a) 0.1M NaCl and (b) without NaCl

Table 3 presents the Tafel fitting results of the polarization curves shown in Fig. 9. The corrosion current densities (I_{corr}) were calculated according to Stern-Geary equation [3]:

$$I_{corr} = \frac{\beta_a \beta_c}{2.3(\beta_a + \beta_c)} \frac{1}{R_p} \qquad (3)$$

Where βa and βc were the Tafel slops of the anodic and cathodic curves, respectively, and R_p was the polarization resistance obtained using the weak polarization fitting which was scanning in the range of ±25 mV versus OCP and not plotted in this paper. These results reveal that (i) for the covered samples, the controlling step was anodic dissolution procedure; (ii) while for the substrates of AZ31, the controlling step was the combination of both anodic and cathodic reactive [23]. Compared with the freshly prepared specimens, the E_{corr} of the covered specimen shifted from -1.55 V_{SCE} to -1.46 V_{SCE}, which was related to the covered layer due to the anodic process by.

Table 3. The Tafel fitting results of the polarization shown in Fig. 9

		β_a (V/unit)	β_c (V/ unit)	R_p (Ω)	E_{corr} (V_{SCE})	I_{corr} (μA/cm^2)
With NaCl	Covered	0.75±0.09	0.13±0.01	1607±100	-1.55±0.02	9.4
	Substrate	0.10±0.02	0.16±0.02	611±46	-1.46±0.05	14.1
Without NaCl	Covered	0.47±0.06	0.24±0.01	4076±86	-1.50±0.04	5.4
	Substrate	0.30±0.03	0.27±0.07	3719±65	-1.47±0.06	5.2

To better understand the protective performance of the corrosion products layer for magnesium alloy against the attack of aggressive species, the ratio parameter (k) was introduced and defined as follows:

$$k_m = \frac{Covered}{Substrate} \qquad (4)$$

where the subscript m was β_a or β_c, which meant the ratio of the Tafel slops of the two type samples. The process would be hindered, when k > 1, and the process be enhanced, when k < 1. In the solution containing NaCl, the products formed on the exposed AZ31 could hinder the anodic dissolution distinctly ($k_{\beta a}$ = 7.5), but the effect on the hydrogen evolution reactive was negligible ($k_{\beta c}$ = 0.82). The ratio parameter was close to 1 ($k_{\beta a}$ = 1.6 and $k_{\beta c}$ = 0.89) for the layer in the medium without Cl^-; the protectiveness of the layer was insignificant, , which could also be confirmed by the curves plotted in Fig. 9(b). Comparing the polarization curves in Fig. 9, it is concluded that the Cl^- was prone to damage the protective layer.

3.4.2 Electrochemical impedance spectroscopy (EIS)

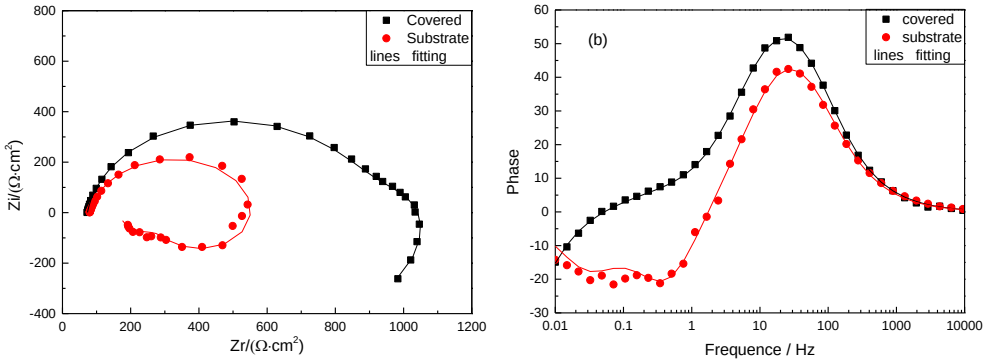

Figure 10. The electrochemical impendence spectroscopy of the tested specimens exposed in the solution containing 0.1 M NaCl: (a) the Nyquist diagram; (b) the Bode phase diagram

Fig. 10 presents the electrochemical impendence spectroscopies of covered samples and AZ31 substrates after immersion in saturated $Mg(OH)_2$ solution with 0.1M NaCl for 30 minutes. The Nyquist diagrams (Fig. 10(a)) reveal that there were three time constants in the electrochemical system, which were as well reflected in the Bode diagram (Fig. 10(b)). The spectra of both substrate and rusted specimens exhibit a capacitive loop in the high frequency range. The high frequency arc was related to the metal dissolution in the corrosion process, whose diameter was associated with the charge-transfer resistance (the corrosion resistance) and the EIS of the rusted samples had larger diameter. [3, 22]. According to the Nyquist diagram of the covered samples, an capacitive arc appeared at the intermediate frequencies, which was caused by the corrosion product layer[2]. An inductive loop appeared at the low frequency region in the EIS of the exposed alloys, while two inductive arcs appeared at this range for the uncovered AZ31 specimen. Such inductive arcs were found in many corrosion studies, and several explanations had been proposed, mainly involving a potential-dependent adsorption of intermediate or electrically active species, such as Mg^+ [1, 3].

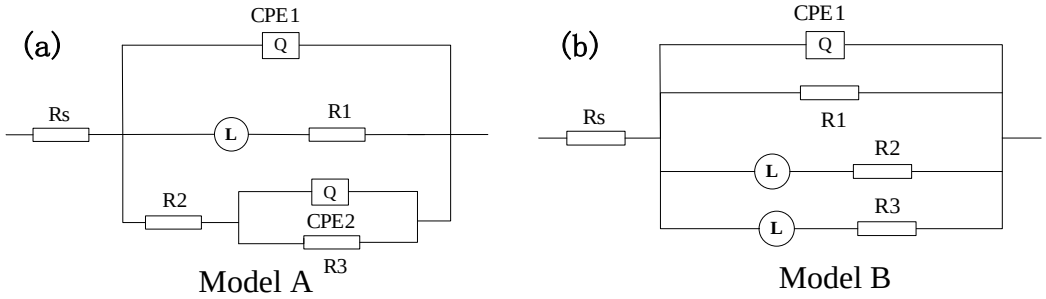

Figure 11. Equivalent circuit models proposed for the system in the experiment: (a) for the covered AZ31; (b) for the AZ31 substrate

Several models had been suggested to fit the EIS data of magnesium alloys in the system containing chloride ions, and the Models [1-3] shown in Fig. 11 was chosen to obtain the best fitting results. The model A was used for the covered specimens (Fig. 11(a)), while model B for the substrate EIS data (Fig. 11(b)). The fitting results were listed in Table 4. The constant phase element (CPE) was selected on behave of the capacitive arc; the inductance was indicated using 'L' and 'R' for the resistance in the equation circles. The fitting values of the elements disclosed that in both models CPE1 was for the interface electrical double layers, and the charge-transfer resistance was represented by R1. The values of R1 for two kinds of samples confirmed that the corrosion products hindered the metal dissolution. What's more, the inductance of the covered specimens was several tens of times larger than that of the substrate one, which uncovered that the process of the intermediate (Mg^+ et.al) changing to the final state (Mg^{2+} et.al) was obstructed.

Table 4. The EIS fitting results using the models shown in Fig. 11 for the tested samples exposed in the solution containing Cl^-

	CPE1		*R*1	CPE2		*R*2	L	R3
	$Y_0(10^{-5}\Omega^{-1}cm^{-2}s^{-n})$	n	(Ωcm^2)	$Y_0(\Omega^{-1}cm^{-2}s^{-n})$	n	(Ωcm^2)	(10^4 Hcm^2)	(Ωcm^2)
Covered	4.59	0.91	821	0.0044	0.7	187	4.95	137
	CPE1		*R*1	L1		R2	L2	R3
	$Y_0(10^{-5}\Omega^{-1}cm^{-2}s^{-n})$	n	(Ωcm^2)	(Hcm^2)		(Ωcm^2)	(Hcm^2)	(Ωcm^2)
Substrated	5.16	0.90	500	236.5		387.5	1469	147.9

4. DISCUSSION

When the magnesium was exposed to the atmosphere, an oxide layer that had the ability against corrosion would form on the surface, which consists of $Mg(OH)_2$, MgO and trace amount of $MgCO_3$ [2]. However, the film would be destructed by the aggressive species in the environment, such as chloride ions, via the chemical and electrochemical methods, during the long-term exposure. Previous paper [11] had reported that the electrochemical reactive was hampered and the chemical process was enhanced in the higher temperature and lower relative humidity condition. Therefore, in the atmospheric environment like Turpan, the chemical evolution might be the main failure mode.

According the morphology and the composition analysis, the magnesium alloy AZ31 degraded through intergranular corrosion (Fig. 4). Fig. 12 presents the corrosion procedure schematic diagrams of AZ31 during exposure under the hot and dry atmospheric environment. At the initial stage, the brucite, $Mg(OH)_2$, firstly formed on the surface, and then transformed into $MgCO_3$ by reacting with CO_2 (Fig. 12(a)), considering $Mg(OH)_2$ could only be stable at low CO_2 pressures [11, 24]. Then, a very thin liquid film that had larger solution resistance condensed on the surfaces of the samples. In this case, the reaction shown in the Fig. 12(b) took place, since the CO_2 pressure in the region was not enough to maintain it [24].

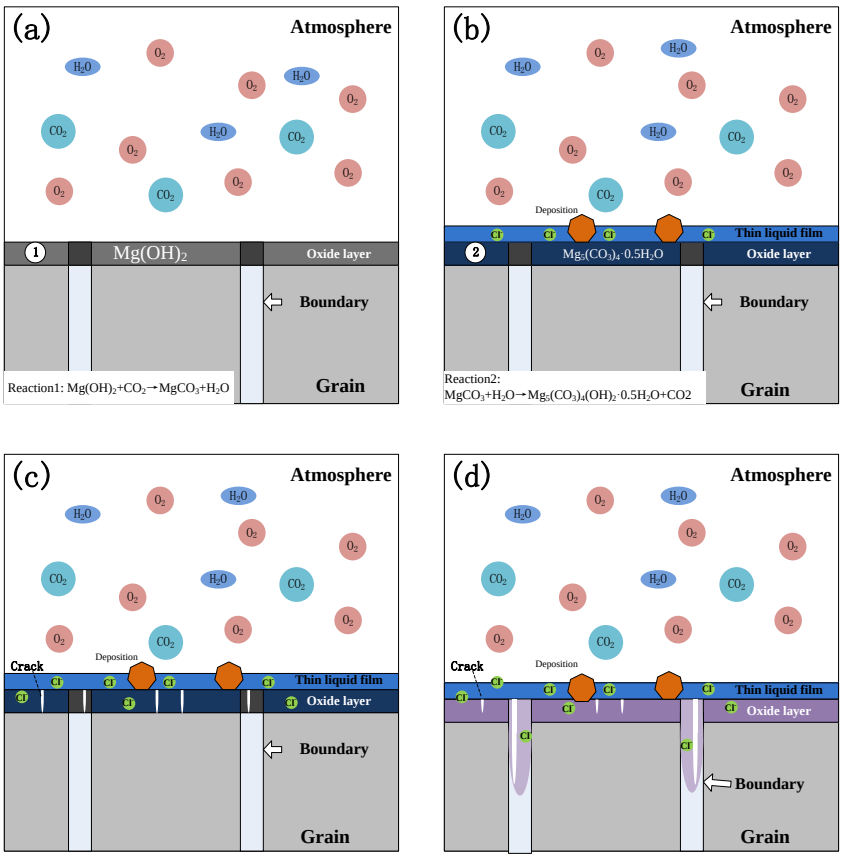

Figure 12. The corrosion process diagram of the magnesium alloy AZ31 during exposure time in Turpan atmospheric environment: (a) the initial exposure stage; (b) the stage that the thin liquid film formed and the oxide layer transformed; (c) the stage that Cl- permeated the layer and some microcracks appeared; (d) the stage that the crack expanded along the crystal boundary.

The inference was obtained based on that the characteristic peaks of $MgCO_3$ or $MgCO_3 \cdot 3H_2O$ were not found in the XRD pattern (Fig. 5). The aggressive species, for example Cl^-, reached to the surfaces of the samples and penetrated into the corrosion layer. Consequently, those aggressive species attacked the sample at the boundaries which was more sensitive to corrosion by means of chemical processes. With the corrosion proceeding, the corrosion rate decreased for the increasing aluminum content in the protective layer [12].

4. CONCLUSION

The corrosion behavior of magnesium alloy AZ31 in the hot and dry atmospheric environment was investigated in Turpan. The morphology and composition of the corrosion product were analyzed with SEM, XRD and XPS. The action mechanism of the corrosion products layer was investigated using the electrochemical methods, The corrosion process was discussed. Through the analyses, the conclusions were:

(1) During the exposure time, the electrochemical process was hindered and the chemical reactive was the primary mechanism that took place in the corrosion system, because of the hot and dry atmospheric environment. It could be obtain from the morphology of AZ31 after removing the rusts that intergranular corrosion occurred severely on the exposed alloys.

(2) The dominate product formed on magnesium alloy during the exposure time was $Mg_5(CO_3)_4(OH)_2 \cdot 0.5H_2O$, and trace amount of Al_2O_3.had also been found. The Al/Mg ratio of the product was several times than that of the substrate.

(3) The electrochemical measurements revealed that the influence of the layer mainly on the metal anodic dissolution procedure and the process of the intermediate changing to the final state.

ACKNOWLEDGMENTS

This work is supported by the National Environmental Corrosion Platform (NECP), the National Natural Science Foundation of China (No. 51222106), the Fundamental Research Funds for the Central Universities (No. 230201306500002) and National Basic Research Program of China (973 Program) (No. 2014CB643300).

Reference

1. L. Feng, Y. W. Song, D. Y. Shan, E. H. Han, Transactions of Nonferrous Metals Society of China, 20 (2010) s638.
2. Z. Cui, X. Li, K. Xiao, C. Dong, *Corrosion Science*, 76 (2013) 243.
3. A. Pardo, M.C. Merino, A.E. Coy, F. Viejo, R. Arrabal, S. Feliú, *Electrochimica Acta*, 53 (2008) 7890.
4. A. Shashikala, R. Umarani, S. Mayanna, A. Sharma, *nternational Journal of Electrochemical Science*, 3 (2008) 993.
5. H. Tang, T. Xin, F. Wang, *International Journal of Electrochemical Science*, 8 (2013) 8115.
6. E. Sherif, A.A. Almajid, *nternational Journal of Electrochemical Science*, 6 (2011) 2131.
7. M. Jönsson, D. Persson, C. Leygraf, *Corrosion Science*, 50 (2008) 1406.
8. S. Feliu, A. Pardo, M.C. Merino, A.E. Coy, F. Viejo, R. Arrabal, *Applied Surface Science*, 255 (2009) 4102.
9. R. Lindström, L.G. Johansson, G.E. Thompson, P. Skeldon, J.E. Svensson, *Corrosion Science*, 46 (2004) 1141.
10. W. Bai, J. Yu, Y. Yang, Y. Ye, J. Guo, Y. Zhang, *nternational Journal of Electrochemical Science*, 8 (2013) 3441-3453.
11. G. Song, S. Hapugoda, D. St John, *Corrosion Science*, 49 (2007) 1245.
12. R.C. Zeng, J. Zhang, W.J. Huang, W. Dietzel, K.U. Kainer, C. Blawert, W. Ke, T*ransactions of Nonferrous Metals Society of China*, 16 (2006) s763.
13. G. Ballerini, U. Bardi, R. Bignucolo, G. Ceraolo, *Corrosion Science*, 47 (2005) 2173-2184.

14. M. Jönsson, D. Persson, Corrosion Science, 52 (2010) 1077.
15. Y. L. Cheng, T. W. Qin, H. m. Wang, Z. Zhang, *Transactions of Nonferrous Metals Society of China*, 19 (2009) 517.
16. L. Huiyan, F. Yuehua, X. Kui, G. Chunyun, D. Chaofang, L. Xiaogang, C*orrosion Engineering, Science and Technology*, 35 (2014) 1098.
17. L.J. Yang, Y.F. Li, Y.H. Wei, L.f. Hou, Y.G. Li, Y. Tian, *Corrosion Science*, 52 (2010) 2188.
18. L. Huiyan, F. Yuehua, X. Kui, G. Chunyun, D. Chaofang, L. Xiaogang, *Corrosion Engineering, Science and Technology*, 26 (2014) 407.
19. Z.Y. Cui, K. Xiao, C.F. Dong, T.Y. Cui, X.G. Li, J*ournal of University of Science and Technology Beijing*, 36 (2014) 339.
20. G.L. Song, Z. Xu, *Electrochimica Acta*, 55 (2010) 4148.
21. Z.Y. Cui, X.G. Li, K. Xiao, C.F. Dong, Z.Y. Liu, L.W. Wang, *Corrosion Engineering, Science and Technology*, 49 (2014) 363.
22. L. Wang, T. Shinohara, B.P. Zhang, *Journal of Alloys and Compounds*, 496 (2010) 500.
23. H. Zhang, Y.L. Zhao, Z.D. Jiang, *Materials Letters*, 59 (2005) 3370.
24. W. White, *Environmental Geology*, 30 (1997) 46.